Assessment of wood microstructural changes after one-stage thermo-hydro treatment (THT) using X-ray computed tomography

Vladimirs Biziks*, Jan Van den Bulcke, Juris Grinins, Holger Militz, Bruno Andersons, Ingeborga Andersone, Jelle Dhaene and Joris Van Acker

***Corresponding author: Vladimirs Biziks**, Latvian State Institute of Wood Chemistry, 27 Dzerbenes str., Riga 1006, Latvia, Phone 0037126099416, Fax: 0049-551-399646; e-mail: orkaans79@inbox.lv

Jan Van den Bulcke: UGCT - Woodlab-UGent, Laboratory of Wood Technology, Department of Forest and Water Management, Faculty of Bioscience Engineering, Ghent University, Coupure Links 653, 9000 Ghent, Belgium; UGCT, University of Ghent Center of X-ray Tomography, Proeftuinstraat 86, 9000 Ghent, Belgium

Bruno Andersons: Latvian State Institute of Wood Chemistry, 27 Dzerbenes str., Riga 1006, Latvia

Ingeborga Andersone: Latvian State Institute of Wood Chemistry, 27 Dzerbenes str., Riga 1006, Latvia

Jelle Dhaene: UGCT - Department of Physics and Astronomy, Faculty of Sciences, Ghent University, Proeftuinstraat 86, 9000 Ghent, Belgium

Joris Van Acker: UGCT - Woodlab-UGent, Department of Forest and Water Management, Faculty of Bioscience Engineering, Ghent University, Coupure Links 653, 9000 Ghent, Belgium; UGCT, University of Ghent Center of X-ray Tomography, Proeftuinstraat 86, 9000 Ghent, Belgium

Juris Grinins: Latvian State Institute of Wood Chemistry, 27 Dzerbenes str., Riga 1006, Latvia

Holger Militz: Wood Biology and Wood Product, Burckhardt-Institute, Georg-August University of Göttingen, Büsgenweg 4, 37077 Göttingen, Germany

Abstract

Microstructural changes in a selection of soft- and hardwoods resulting from thermo-hydro treatment (THT) at 160°C were examined using a state-of-the-art micro CT scanner developed at the Ghent University Center for X-ray Tomography (UGCT). A dedicated X-ray scanning and volumetric processing protocol was developed. All reconstructed volumes had approximate voxel pitches of between 0.8–1.2 μm^3. The microstructures of the same needle-shaped specimens before and after THT were visualized, and individual parameters (maximum opening and lumen volume) for various cell types were quantified and compared. The highest values of wood substance volume were recorded for the ash sapwood and spruce specimens: 81% and 72%, respectively. A significant correlation between the wood substance gravimetrical mass loss and the X-ray volume loss after THT was found. When evaluating individual fiber parameters, the largest change was found in the lumen volume of several tissue component types (libriform, tracheid and ray parenchyma). The average volume reduction for the aspen fiber lumen after THT was 31%, a value 2.6 times higher than the volume reduction of the average vessel lumen. These results show that THT causes changes to the macroporosity and individual parameters of both soft- and hardwoods. Significant differences in porosity were observed between wood specimens. The porosity of ash sapwood increased from 41% to 56%, whereas the porosity of birch decreased from 34% to 29%. These results indicate that strength of interaction between the different types of fibers take place. Additionally, the results show that wood species with less cell wall material (with higher initial porosity) tend to exhibit large microstructural changes, such as large decreases in total cell wall material volume. This is true for gray alder and ash sapwood, possibly due to increased heat and mass transfer during THT. Porosity increased for wood species with smaller amounts of cell wall material after THT (e.g., spruce and ash sapwood) because there was less shrinkage but an equal loss of cell wall material. Thus, the microstructural changes of THT wood can be investigated by quantifying changes in wood volume, porosity and individual parameters using X-ray CT scanning.

Keywords: Thermo-hydro treatment; Mass loss; X-ray Computed Tomography; Wood Microstructure; Cell wall material; Porosity

Introduction

The thermal modification (TM) of wood is principally based on chemically transforming cell wall components by inducing autocatalytic reactions through the use of heat, pressure and water (Dietrichs *et al*. 1978; Grinins *et al*. 2013); this process causes shrinkage and mass loss, irreversibly transforming the wood's microstructure. The extent of these modifications depends on the initial chemical composition and microstructure of the wood, the treatment atmosphere (saturated or superheated steam, nitrogen, air or hot oil) and other process parameters (temperature, duration, and pressure) (Zaman *et al*. 2000). In the most recent decade, several new TM processes have been developed by Wood Treatment Technology (WTT) in Denmark, Vacuu^3 (Opel-Thermo) in Germany, and FirmoLin in the Netherlands. The main difference between one-stage THT and the Plato process is that several steps (hydrothermolysis, drying, and partial curing) have been combined, allowing the treatment to be conducted within a single piece of equipment (autoclave).

Scanning electron microscopy (SEM) and light microscopy (LM) have been used to investigate the surface of individual treated wood cells. These studies showed that the cell wall thickness and lumen diameter are decreased, cell wall breakages occur near vessels and rays, and the morphological and structural integrity is generally diminished (Fengel 1966; Filló and Peres 1970; Boonstra et al. 2006). It is therefore essential to observe the structure before and after treatment to assess the effect of treatment and to enable the comparison of different treatments.

SEM and LM provide only limited information on the 3D structure of thermally treated wood. However, X-ray computed tomography (CT) and accompanying image analysis have been used successfully to characterize the 3D microstructure of wood, and the application of this technique in the field is broadening. Van den Bulcke et al. (2009; 2013) illustrated the power of X-ray CT as a tool for analyzing wood anatomy at both the descriptive and quantitative levels and were able to resolve sub-micron details using 3D reconstructions. As a non-destructive technique, X-ray CT avoids potential artifacts introduced by sample preparation, which is a key advantage for monitoring and quantifying the effect of wood treatment on the same specimen.

In this study, needle-shaped specimens from a selection of soft- and hardwoods were scanned using the X-ray µCT Nanowood scanner at UGCT, which focuses on visualizing and quantifying 3D microstructural changes resulting from THT. The aim of this study was to

assess the general microstructural changes in soft- and hardwood tissue elements resulting from THT.

Materials and methods

Sample description

The effects of THT on the wood microstructure of birch (*Betula pendula*), aspen (*Populus tremula*), grey alder (*Alnus incana*), ash (*Fraxinus excelsior*) early- (EW) and latewood (LW), spruce (*Picea abies*) and Scots pine (*Pinus sylvestris*) were assessed. To obtain data of high quality and high resolution, small specimens were used. Samples were prepared from larger blocks and subdivided using a scalpel into needle-shaped specimens measuring approximately 0.4 x 0.4 x 6 mm. Specimens were oven-dried and stored in a desiccator to avoid volume fluctuations caused by moisture absorption. The same specimens were scanned before and after the THT regimen at 160°C.

Treatment

THT was carried out using a pilot-scale 560 l stainless steel autoclave produced by WTT. The required temperature was maintained by circulating hot mineral oil in the jacket. The working THT cycle diagram at 160°C comprises three steps (Table 1): (I) heating, (II) 1-h incubation at 160°C, and (III) a final cooling. A known quantity of water that depends on the initial amount of water in the wood and the batch volume was pumped in at the beginning of the process to improve the heat transfer from the autoclave walls and to increase the reactivity of the cell wall components at relatively low temperature. The rate of the process parameters was changed (increased/decreased) during the heating and cooling steps to avoid artificial crack formation in the wood due to incorrect process management. The changes for each step are listed in Table 1.

The mass loss (ML) of the THT needle-shaped specimens was calculated as $m_T\ (\%) = 100(m_0 - m_1)/m_0$ (Eq. 1), where m_T is the ML due to THT, m_0 is the oven-dried mass of the specimen before THT, and m_1 is the oven-dried mass of the specimen after THT. Four replicates were used per species to calculate the average ML.

Data acquisition and analysis workflow

To allow a fair assessment of the microstructural changes resulting from THT, oven-dried untreated and THT-treated specimens were subjected to identical acquisition and analysis procedures.

Image acquisition

All specimens were mounted on a holder, and the central region of all wood samples (approximately 1 mm in height depending on the resolution) was scanned using the Nanowood scanner at the Center for X-ray Tomography at Ghent University (UGCT; http://www.ugct.ugent.be) as described previously (Dierick et al. 2014). The coordinates of the central region were recorded before treatment to enable the same region to be scanned after treatment. This flexible, state-of-the-art scanner is controlled using in-house developed software with a generic interface (Dierick et al. 2010). All needle-shaped wood pieces were scanned at an average voltage of 55 kV, a target current of 160 μA, and an exposure time of 1500 ms per image, resulting in an approximate scan time of 45–60 min per object. Reconstruction was performed using Octopus (Vlassenbroeck et al. 2007), a tomography reconstruction package for parallel and cone-beam geometry, with approximately 20 min per scan. All specimens were filtered using the phase contrast method in Octopus (De Witte et al. 2009; Boone et al. 2009). The resulting high-resolution scans had an approximate voxel pitch of 0.8–1.2 μm^3 with 2^{16} grayscale levels. Reconstructed images of the samples before and after THT were visualized using Octopus Analysis (www.insidematters.be; previously known as Morpho+; Brabant et al. 2011) and rendered in 3D using VGStudio MAX.

Image preprocessing

Preprocessing was performed in Morpho+. For correct analysis, rotation of the volume was necessary such that the three major wood axes (x = tangential, y = radial, z = axial) were aligned properly according to the virtual cross-sectional planes. A reconstructed cross-section of birch is shown in Figure 1a. Bilateral filtering with edge preservation was used to reduce noise (Figure 1b) (Tomasi and Manduchi 1998). The volumes were then binarized, and the volume of interest (VOI) was determined, thus ensuring the same VOI for both the untreated and treated volumes (Figure 1c). Subsequently, the volume was thresholded once more within

the VOI to differentiate air and wood, which enabled calculation of the porosity and the volume of wood tissue. Cell wall porosity is not considered here due to the inherent resolution limitation of X-ray CT and the partial volume effect; therefore, only larger pores (an approximate volume of 1 μm^3 or larger) were detected.

Image segmentation and calculations

Filtered volumes with binarized cell lumens were labeled, distance transformed and separated using the watershed operation, resulting in segmented lumens of different cell types and vessels (Figure 1d). The effects of THT on hard- and softwood were evaluated according to the "good fibers/good vessels" principle. A fiber or vessel lumen is considered good when clearly separated and not connected with the lumens of other fibers or vessels. Split lumens, due to over-segmentation, were rejoined manually. Through careful visual selection, we were able to locate the same cells (vessels, libriforms, tracheids…) in both the untreated and treated volumes. Examples of well-separated vessels and lumens (Figure 1e) and lumens of different birch cell types are shown in Figure 1f. The volumetric changes of the specimens were calculated based on the 3D data, of which a volume rendering is illustrated in Figure 2g.

The total amount of wood tissue (WT) voxels in the VOI (V_{WT}) was calculated according to $V_{WT} = (V_{VOI} - V_L) \times v_p$ (Eq. 2), where V_{VOI} represents the total number of voxels in the VOI, V_L represents the total number of lumen voxels (voids) in the VOI, and v_p represents the approximate voxel pitch.

The porosity within the VOI was calculated according to $Porosity\ (\%) = 100(V_L/V_{VOI})$ (Eq. 3).

The maximum opening was calculated automatically by Morpho+ and was based on a virtual sphere with a maximum diameter that could fit inside the fiber lumen without having any common point (voxel) of contact with the cell wall material (voxel); hence, the maximum opening is the maximum-inscribed sphere in the cell lumen.

Results and discussion

A high-resolution anatomical investigation of the 3D microstructural changes occurring in six wood species as a result of THT was carried out in this study using X-ray CT. Vessel and fiber lumen volumes were analyzed in 3D before and after treatment to quantify the resulting microstructural changes.

Relevant microscopic features of wood species

The average lengths of tracheid and libriform fibers were approximately 3,000 and 1,500- 1,100 µm, respectively. However, the selected height of the specimen was 300 µm; thus, the specimen was too short to compare lumen volume differences between various cell types in hardwoods and tracheids in softwoods. In addition, the changes in the longitudinal direction were small and might be less than the sensitivity of the measurement; therefore, scans of the transversal section were used to assess microstructural changes.

Figure 2 shows a transversal section of the untreated specimen for each wood species. This figure clearly illustrates that X-ray CT is a powerful technique for visualizing anatomical structure (Bugani et al. 2009; Bessières et al. 2013).

During scanning, detectors measure the intensity of the X-ray radiation that is transmitted through the object, and object density is recorded using 256 grey levels. Light colors represent areas with higher densities and dark colors represent areas of lower density. As shown in the initial images of all wood species (Figure 2), light colors were found for pine, birch and ash LW. This result might be explained by their having a lower porosity (Table 2), and hence, a higher cell wall proportion in the initial, lighter VOI image.

Figures 2d and 2g show transversal sections of two softwoods, spruce and pine, consisting mainly of rectangular tracheids. A resin canal is also visible in the pine specimen, as well as the transition zone from early- (EW) to latewood (LW). Large EW-tracheid lumen diameters (or maximum openings) can be differentiated from the smaller ones observed in LW. According to the data (Figure 3g) obtained from lumen segmentation of the pine wood tracheids, the average maximum EW opening ranges from 15 to 19 µm; i.e., 2.5-3 times larger than the LW tracheid lumen, which measured 5-9 µm. Transversal sections of spruce mainly comprised tracheids that were more homogeneous in size (earlywood), mainly with large diameters ranging from 18-26 µm (Figure 3f).

Typical hardwood transversal sections are shown in Figure 3. The anatomical structure comprises various fibrous elements: axial or vertical elements are vessels and libriforms, whereas radial or horizontal elements are rays comprising ray parenchyma cells (Figure 3a; e). Vessels are in solitary arrangement (Figure 3e; b), in pairs (Figure 3f), or in radial multiples of up to four vessels in a row (Figure 3c). Birch, grey alder and aspen are semi-diffuse-porous wood species; the vessels slightly changed in size or distribution from EW to LW. The average vessel lumen diameters are somewhat similar between aspen and grey alder (25-40 µm) (Figure 4a and 4b), and slightly larger for birch wood (40-55 µm) (Figure 4c). In contrast, ash is a ring-porous species, and its vessels significantly change in size and distribution from EW to LW and from pith to bark, i.e., from heartwood (HW) to sapwood (SW). The EW vessel lumen is considerably (3-4 times) larger in diameter (75-110 µm) (Figure 4d) than the LW vessel lumen (20–25 µm) (Figure 4e).

The wood also consists of a compact arrangement of different fiber types, with vessels surrounded by rays and libriform fibers. Differentiating the ray parenchyma from other cell types was not straightforward; therefore, the ray parenchymas were not considered. According to the data presented in the histogram in Figure 3, all hardwood species have a similar distribution of fiber lumen diameters (4-8 µm), with the exception of gray alder (7-11 µm).

Clear micro-structural differences exist among the samples (Figure 3). All of the observations show the possible impact of considerable variability in wood porosity. The initial images were converted into binary images in which black voxels correspond to voids (lumens of different cell types) and white voxels correspond to matter (cell walls). The proportion of matter for a given volume i.e., cell wall proportion or porosity, was obtained. The highest porosity was found for spruce (48%) because it exhibits the largest tracheid diameter. There are fewer vessels in ash early wood than there are in other late woods; however, in this case, the ash EW specimen had similar porosity (41%) to gray alder (42%), aspen (37%) and birch (34%). Therefore, the variability in porosity is related to the cell type (thin- or thick-walled cells). The highest volume of cell wall material is found for ash LW (81%) because it exhibits a rather low concentration of vessels with small vessel diameters. For ash EW and gray alder, the wood volume contents of 59% and 58%, respectively, can be explained by the small number of vessels with large diameters for ash SW and the large number of vessels with small diameters for gray alder. Cell wall material of up to 72% is present in the pine wood sample, which can be explained by the large amount of LW present within a cell wall thickness that is 2 times higher than that of EW and the smaller diameter of the tracheid lumen. The spruce sample, for example, contains 52% wood due to the presence of thin-walled and large-

diameter tracheids. Birch and aspen have nearly the same amount of wood (66% and 63%, respectively). The number of cells obviously plays an important role in porosity, but to a lesser extent. The smallest values of porosity were measured for ash HW (19%) and pine (28%).

In this study, the porosity represents the total air volume (macro-voids) in the specimens, but is not related to the volume distribution occupied by the different cell types. The total void volume in the softwood specimens represents the tracheid lumen. Due to the cell's multiformity in hardwoods, a division can be observed with approximately 2/3 of the macro-void volume belonging to vessels and 1/3 belonging to libriforms and rays for birch, grey alder and aspen. However, large distribution differences in void volume were found between the ash EW and LW specimens. For ash LW, 11% of the void volume comprised vessels and 89% comprised various fiber types, whereas for ash EW, the corresponding values were 73% and 27%, respectively.

Microstructural changes induced by THT

The specimens were subjected to thermo-hydro treatment (THT) in a saturated steam atmosphere in a pilot-scale autoclave at 160°C for 1 h. During the treatment, autohydrolysis (dehydration) of the hemicelluloses occurred, and low molecular weight compounds (acetic and formic acid, furanaldehyde, water) evaporated and were thus removed from the matrix, resulting in mass loss, shrinkage and microstructural changes. The changes recorded after treatment of the needle-shaped specimens were comparable to changes that occur at the surface of larger objects.

The mass loss (ML), porosity and total volume change of the specimen and cell wall material of the THT wood from the different species are listed in Table 2. Slight differences in ML were apparent among the various wood species, both for the softwood (15-19%) and for the hardwood (17–24%). As mentioned previously, the number of wood voxels in the specimen before and after treatment might be related to the weight loss. As shown in Table 2, the total volume loss of cell wall material and the mass loss did not differ greatly between wood species, except for spruce. This result shows the feasibility of using wood voxels as an indicator of wood loss during treatment. Possible differences in the results between mass loss and the loss of wood voxels might be attributed to an increase or decrease of cell wall material during thresholding and to the fact that only a very small part of the sample is scanned, whereas the entire sample is weighed. It is possible that certain regions in the entire needle-

shaped specimen exhibit larger shrinkage and mass loss than that observed in the VOI. The higher ML of hardwoods can be attributed to their having a higher amount of hemicellulose than softwoods, which exhibit the highest susceptibility to thermal decomposition (Bourgois *et al.* 1989).

Visualizing exactly the same region of the specimen before and after THT clearly illustrates the shrinkage (Figure 7). To understand the results, the dimensions of the samples were not physically altered. The top of the gray (= untreated) volumes were virtually cut to show the brown (= treated) sample clearly. Larger shrinkage was observed in the tangential direction than in the radial direction. Generally, all wood specimens exhibited similar reductions in volume of approximately 17% (Table 2); however, for ash EW and spruce, the levels of shrinkage were 2 and 6 times smaller, respectively, than those observed for the other wood species. One explanation for this finding might be related to the total amount of wood or to the wood cell wall thickness. Diffusion and evaporation of low molecular weight compounds occur during the cooling stage. Simultaneously, the free space between the macromolecular constituents gradually decreases, and the matrix is rearranged. Size reduction of single cells might be explained by the fact that the macromolecules continue to interact through various types of bonding. The molecules probably tend to occupy a more energy-efficient layout and distort each other due to plasticity. The distances between the macromolecules decrease, causing single cells to shrink. Cell displacement (equivalent to shrinkage in this case) might occur through the middle-lamella that binds cells together. The amount and distribution of constituents in thin cell walls might be much lower and might result in minor shrinkage of the sample. A different reduction in the size of the cell wall due to THT was observed previously (Biziks et al. 2013). This study found that the effect of treatment differs depending on cell type.

Some diversity exists between different wood species regarding the lumen's maximum opening and volume in different cell wall types after THT treatment. The maximum opening is the maximum inscribed sphere in the tracheid, fiber or vessel lumen. Histograms of maximum diameter and lumen volume of different cell types for each wood specimen before and after THT were plotted and compared. It can be concluded that the vessels barely change as a result of THT. According to Figures 5 and 6, similar reductions in diameter (8-11%) and vessel lumen volume (8-14%) were found after treatment for all hardwoods. The largest effect of the treatment was observed for the different types of wood cells (libriform, tracheid and ray parenchyma). The lumen volume and maximum opening (Figures 3 and 4) differ among wood

species. For example, the reduction in libriform lumen was higher than the reduction of the vessels (2 times higher for birch and 3 times higher for ash EW).

Figures 5 and 6 show that larger or fewer reductions in diameter and lumen volume occurred in all wood specimens, with the exceptions of spruce and ash sapwood. The largest decreases in lumen volume and diameter were observed in birch and aspen. Aspen, gray alder and pine exhibited similar shrinkages in fiber lumen volume and diameter. The ash EW fibers (libriform, ray parenchyma) and spruce tracheid lumen volume and diameter increased after treatment, unlike the results for other specimens.

Additionally, some heterogeneity was observed within the ash EW specimen; vessel size decreased as the fiber lumen (-8) and (+4%) increased. It is possible that the fibers are more compressed in some parts, but are more expanded in other parts of the wood specimen. The anisotropy of cell wall shrinkage induces internal stress, which can be sufficiently large to create microcracks between the cells or even damage the cell wall.

The porosity of a specimen can remain constant before and after the treatment only if the change in volume of the wood cell wall equals the change of the total VOI volume, as was observed for pine and ash HW. The data in Table 2 provide evidence that for all other species, the cell wall and total volume changes differed. Wood substance and shrinkage (total volume change) were well-correlated. Species with less cell wall material, such as alder, ash EW and spruce, exhibited higher porosity after THT than species such as birch and aspen. The former shrank less than the latter but exhibited nearly the same weight loss of wood.

Conclusions

X-ray micro-CT was found to be a convenient 3D method for characterizing wood microstructural changes caused by THT and enabled the visualization and quantification of shrinkage. Analysis of X-ray data from the initial specimen's volume showed that the volume occupied by the cell wall material clearly differed among wood species.

The vessel lumen volume and maximum opening changes after THT were similar among hardwood species, decreasing by approximately 8% and 12%, respectively.

The largest differences between the parameters of individual morphological elements resulting from THT were observed between different cell types (libriform, tracheid and ray parenchyma). The fiber lumen volume and maximum opening differed among species; however, the volume reduction was generally 2 to 4 times higher for fiber lumen than for vessels.

Specimen porosity after THT was also investigated and differed significantly among species, indicating that different interactions occur among different fiber types. The decrease in porosity can be used as a process quality indicator. During treatment, wood fibers pass through several dimensional changes at the microstructural level (cell wall swelling and shrinkage); therefore, sufficient time should be allowed for the wood matter to adjust to these changes. The porosity data show that the same parameter process rate cannot apply to all wood species. In wood specimens of lower density (e.g., alder or ash EW), the same heating and cooling rates resulted in a porosity increase that impaired the final product's properties (e.g., mechanical strength, water absorption rate and penetration depth).

The X-ray CT and image processing protocol used to examine the effect of the thermal treatment of wood presented in this study can be used for many other purposes involving the evaluation of certain treatments; i.e., dynamic processes that occur in wood can be evaluated (e.g., the rate of cell wall penetration or "bulking").

Acknowledgements

The authors express their appreciation to COST Action FP0802, FP0904 and FP1006, and specifically its chairs Professor Karin de Borst, Professor Parviz Navi and Dr. Stefanie Wieland for providing financial support for the STSMs. We also thank all of the members of the Laboratory of Wood Technology (Woodlab) at the Faculty of Bioscience Engineering at Ghent University (UGent) for their help.

References

Biziks, V., Andersons, B., Beļkova, L., Kapača, E., Militz, H. (2013) Changes in the microstructure of birch wood after hydrothermal treatment. Wood Sci. Technol. 47:717–735.

Boone, M., De Witte, Y., Dierick, M., Van den Bulcke, J., Vlassenbroeck, J., Van Hoorebeke, L. (2009) Practical use of the modified Bronnikov algorithm in micro-CT. Nucl. Instrum. Methods Phys. Res. Sect. B: Beam Interact. Mater. At. 267:1182–1186.

Boonstra, M.J., Tjeerdsma, B.F. (2006) Chemical analysis of heat-treated softwoods. Holz. Roh. Werkst. 64:204–221.

Bourgois, J., Bartholin, M., Guyonnet, R. (1989) Thermal treatment of wood: Analysis of obtained product. Wood Sci. Technol. 23:303-310.

Brabant, L., Vlassenbroeck, J., De Witte, Y., Cnudde, V., Boone, M.N., Dewanckele, J., Van Hoorebeke, L. (2011) Three-dimensional analysis of high-resolution X-ray computed tomography data with Morpho+. Microsc. Microanal. 17:252–263.

Bugani, S., Modugno, F., Łucejko, J.J., Giachi,G., Cagno, S., Cloetens, P., Janssens, K., Morselli, L. (2009) Study on the impregnation of archaeological waterlogged wood with consolidation treatments using synchrotron radiation microtomography. Anal Bioanal. Chem. 395:1977-1985.

Davis, J., Wells, P. (1992) Computer tomography measurements on wood. Ind. Metrol. 2(3-4):195-218.

De Witte, Y., Boone, M., Vlassenbroeck, J., Dierick, M., Van Hoorebeke, L. (2009) Bronnikov-aided correction for X-ray computed tomography. J. Opt. Soc. Am. A-Opt. Image Sci. Vis. 26:890–894.

Dierick, M., Van Loo, D., Masschaele, B., Boone, M. and Van Hoorebeke, L. (2010) A LabVIEW® based generic CT scanner control software platform. J. X-ray Sci. Technol. 18:451–461.

Dierick, M., Van Loo, D., Masschaele, B., Van den Bulcke, J., Van Acker, J., Cnudde, V., Van Hoorebeke, L.(2014) Recent scanner developments at UGCT Nucl. Instrum. Methods Phys. Res. Sect. B: Beam Interact. Mater. At. 324:35-40.

Dietrichs, H.H., Sinner, H., Puls. J. (1978) Potential of steaming hardwoods and straw for feed and food production. Holzforschung 32:193–199.

Derome, D., Zillig, W., Carmeliet, J. (2012) Variation of measured cross-sectional cell dimensions and calculated water vapor permeability across a single growth ring of spruce wood. Wood Sci. Technol. 46:827–840.

Fengel, D. (1966) On the changes of the wood and its components within the temperature range up to 200°C – Part 2. Holz Roh-Werkst. 24: 98–109.

Filló, Z., Peres, T. (1970) *Holztechnologie* 11, 270-273. *Cited in Fengel and Wegener* (1989).

Goring, D.A.I. (1963) Thermal Softening of Lignin, Hemicellulose and Cellulose. Pulp and Paper Magazine of Canada. 517–527.

Grinins, J., Andersons, B., Biziks, V., Andersone, I., Dobele, G. (2013) Analytical pyrolysis as an instrument to study the chemical transformations of hygrothermally modified wood. Journal of analytical and applied pyrolysis. 103:36–41.

Mitchell, M.D., Denne, M.P. (1997) Variation in density of *Picea sitchensis* in relation to within-tree trends in tracheid diameter and wall thickness. Forestry 70: 47–60.

Polge, H. 1965. Study of wood density variations by densitometric analysis of X-ray negatives of samples taken with a Pressler auger. Paper presented at meeting of IUFRO 41, Oct, 1965. pp. 19

Van den Bulcke, J., Boone, M., Van Acker, J., Stevens, M., Van Hoorebeke, L. (2009) X-ray tomography as a tool for detailed anatomical analysis. Ann. For. Sci. 66:508.

Van den Bulcke, J., Biziks, V., Andersons, B., Mahnert, K.C., Militz, H., Van Loo, D., Dierick, M., Masschaele, B., Boone, M., Brabant, L., De Witte, Y., Vlassenbroeck, J., Van Hoorebeke, L., Van Acker, J. (2013) The potential of X-ray computed tomography for 3D anatomical analysis and microdensitometrical assessment in wood research with focus on wood modification. International Wood Products Journal 4:183-190.

Vlassenbroeck J., Dierick M., Masschaele B., Cnudde V., Van Hoorebeke L., Jacobs P. (2007) Software tools for quantification of X-ray microtomography at the UGCT. Nucl. Instrum. Meth. Phys. Res. A. 580:442–445.

Zaman, A., Alén, R., Kotilainen, R. (2000) Heat behaviour of *Pinus sylvestris* and *Betula pendula* at 200 - 230°C. Wood Fiber Sci. 32:138-143.

Table 1. Characteristic parameters of the hydrothermal treatment working cycle at 160°C.

Treatment step	**Total step duration (min)**	**Temperature range (°C)**	**Duration (min)**	**Temperature change rate (°C min^{-1})**	**Pressure range (N*mm^{-2})**	**Duration (min)**	**Pressure Change rate (N*mm^{-2} *min^{-1})**
I (heating)	600	r.t.*-140°	600	0.23-0.24	0.62	250	0.0025
II (holding)	60	constant 160°	60	constant	0	60	constant
III (cooling)	540	T_{max} to 40°	540	0.22-0.23	0.62	300	0.00206

*r.t. – room temperature (20°C)

Table 2. VOI characterization after hydrothermal treatment as calculated based on X-ray tomography scans.

Wood species	Mass loss* (%)	Change in total volume of cell wall material (%)	Change in total volume (%)	Porosity before treatment (%)	Porosity after treatment (%)
Gray alder	16	-19	-17	42	46
Aspen	21	-16	-18	37	32
Birch	16	-17	-19	34	29
Ash sapwood	24	-19	-9	41	56
Ash heartwood	15	-17	-16	19	16
Pine	15	-17	-17	28	28
Spruce	16	-8	-3	48	54

*Mass loss is calculated gravimetrically

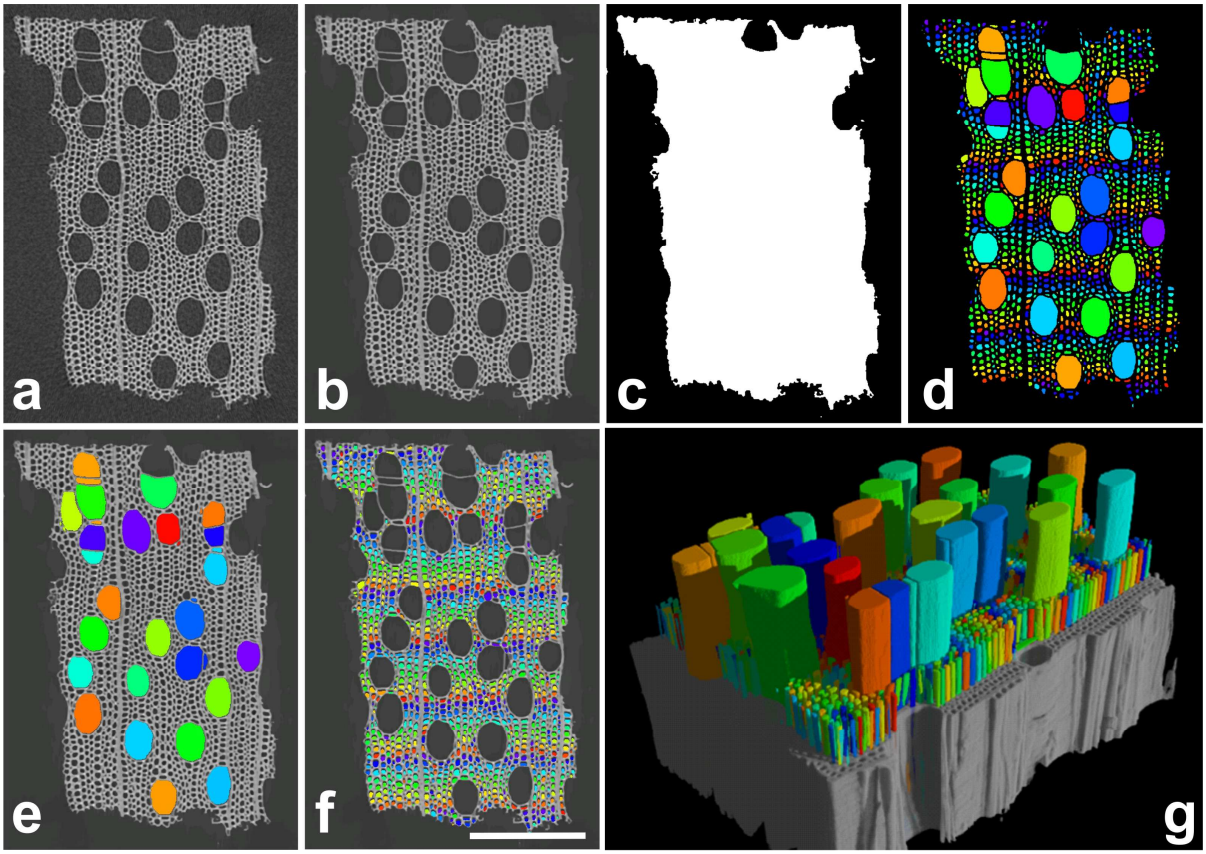

Figure 1.

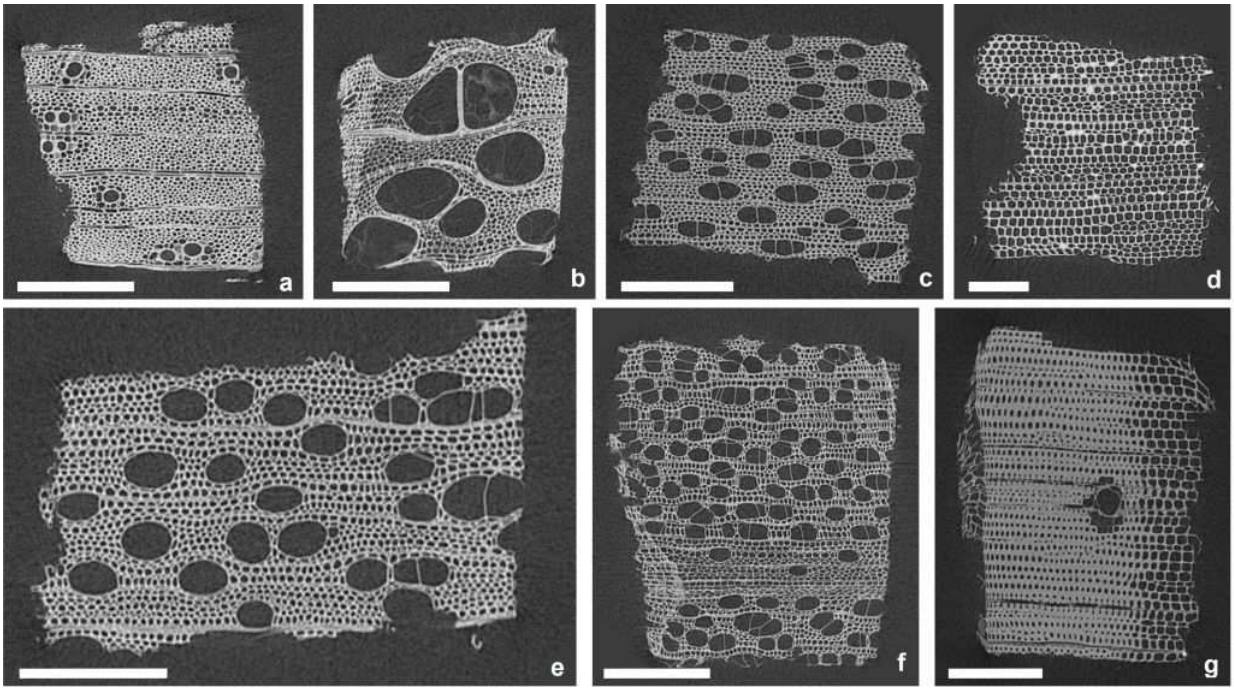

Figure 2.

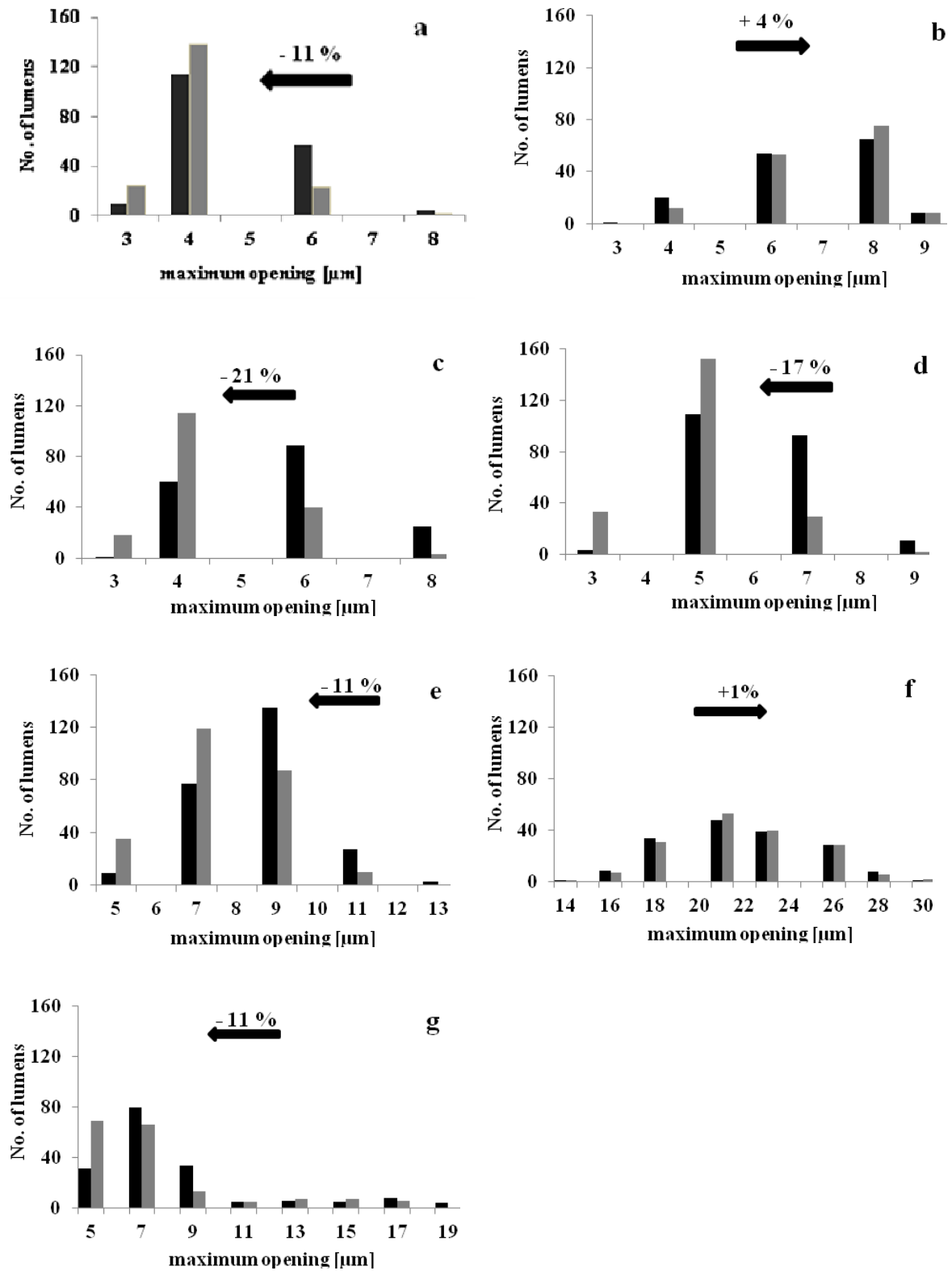
a
- 11 %
No. of lumens
maximum opening [µm]
b
+ 4 %
No. of lumens
maximum opening [µm]
c
- 21 %
No. of lumens
maximum opening [µm]
d
- 17 %
No. of lumens
maximum opening [µm]
e
- 11 %
No. of lumens
maximum opening [µm]
f
+1%
No. of lumens
maximum opening [µm]
g
- 11 %
No. of lumens
maximum opening [µm]

Figure 3.

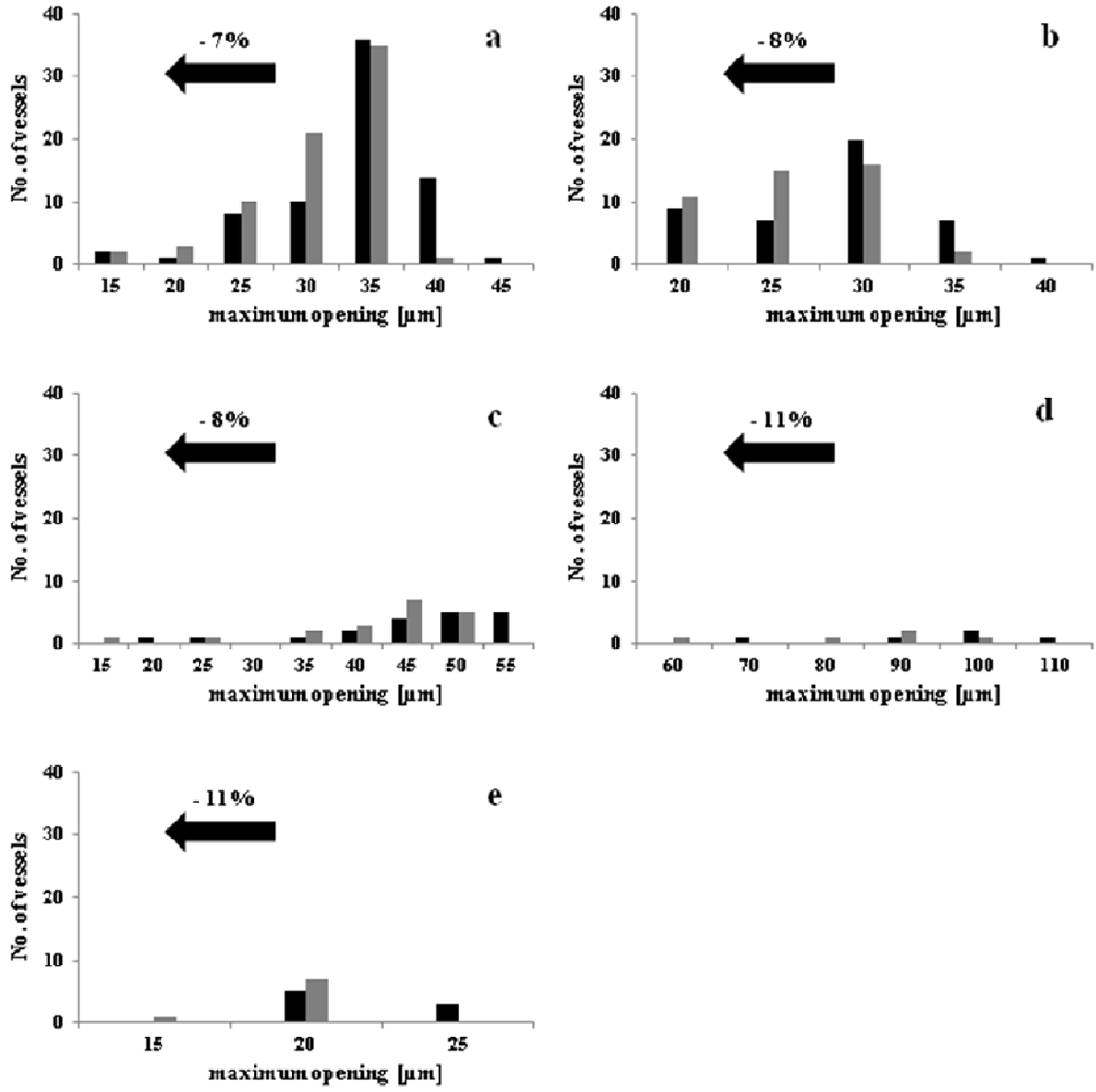
a
- 7%
No. of vessels
maximum opening [µm]
b
- 8%
No. of vessels
maximum opening [µm]
c
- 8%
No. of vessels
maximum opening [µm]
d
- 11%
No. of vessels
maximum opening [µm]
e
- 11%
No. of vessels
maximum opening [µm]

Figure 4.

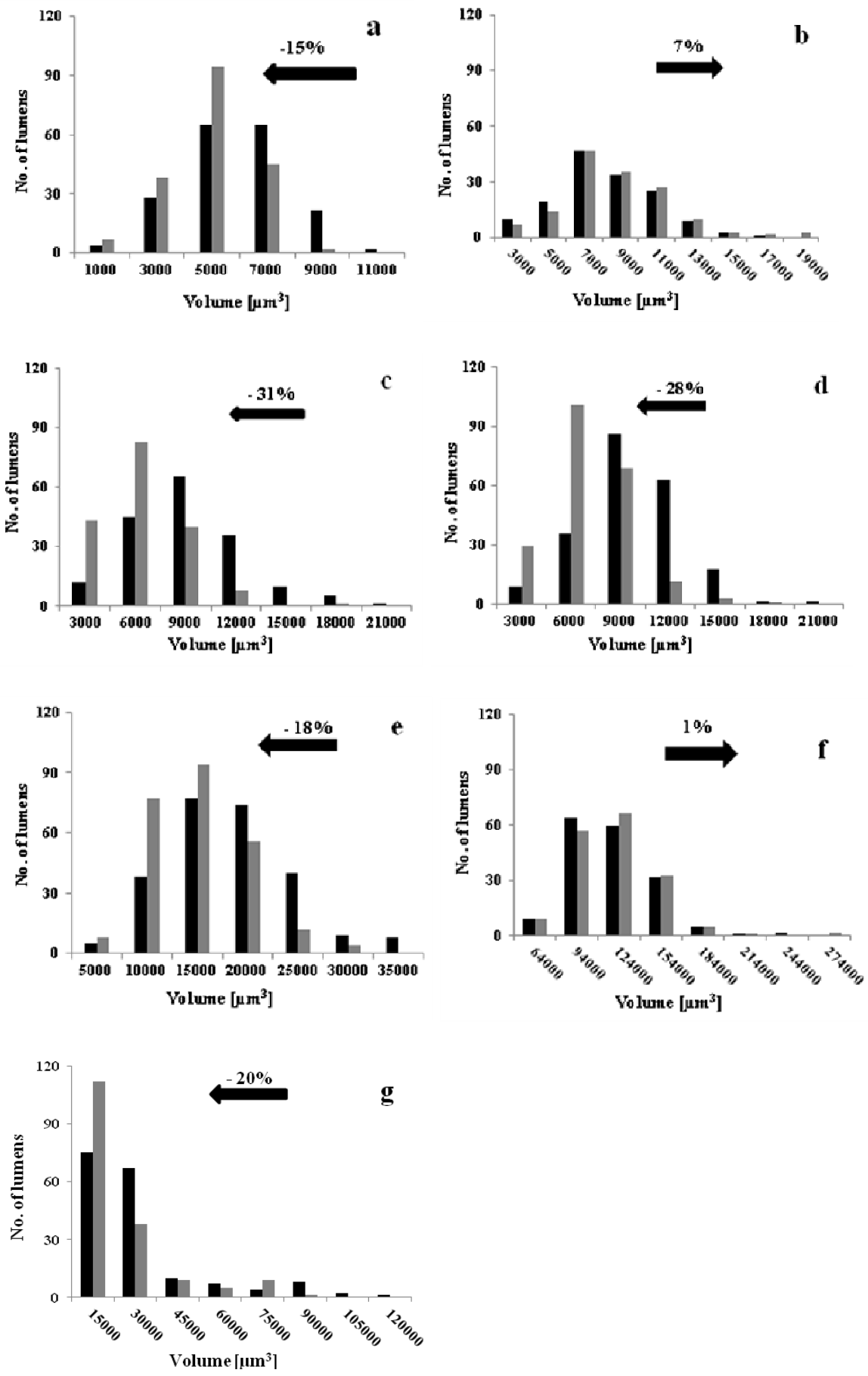

Figure 5.

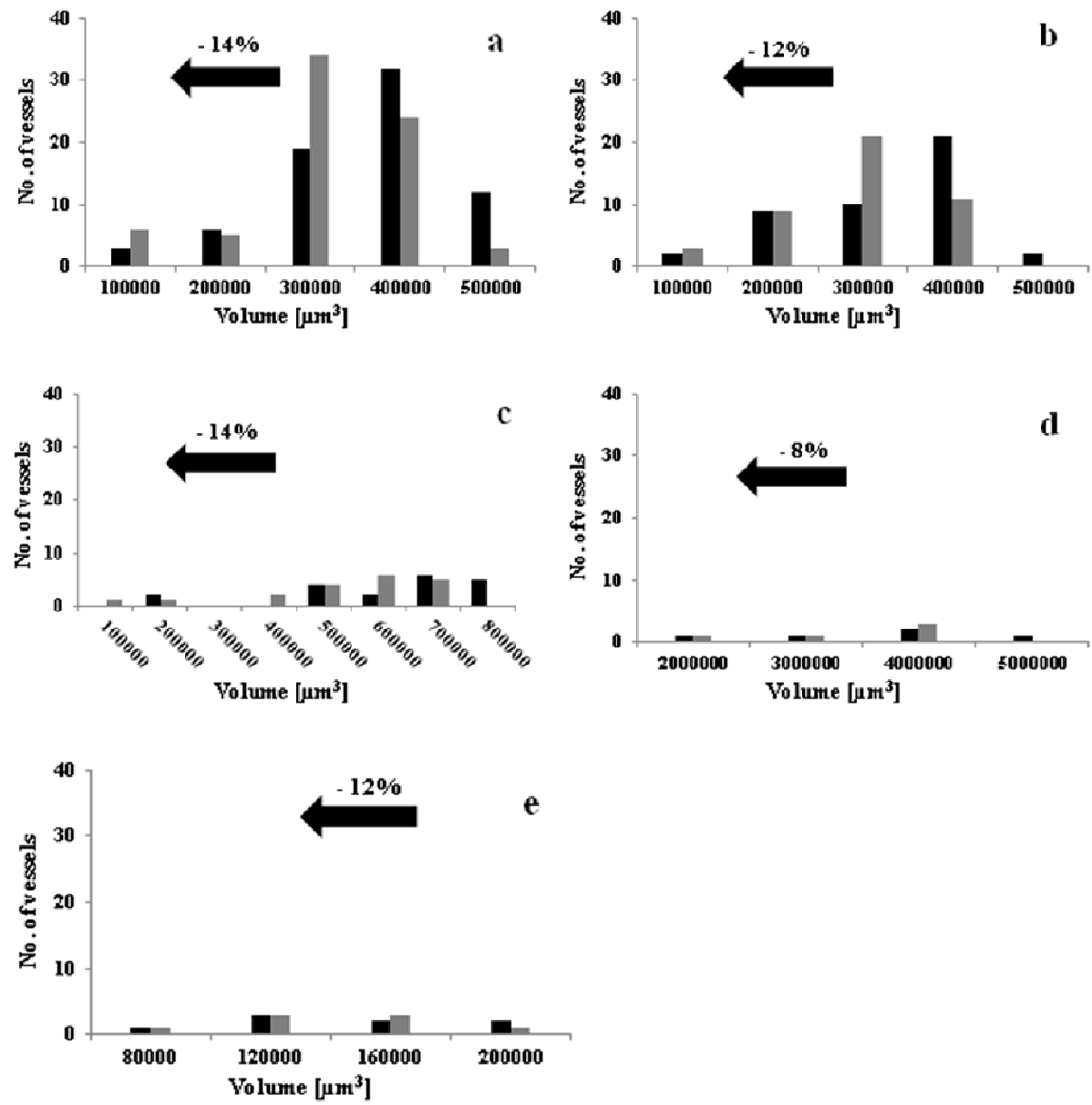
a
- 14%
No. of vessels
Volume [µm³]
b
- 12%
No. of vessels
Volume [µm³]
c
- 14%
No. of vessels
Volume [µm³]
d
- 8%
No. of vessels
Volume [µm³]
e
- 12%
No. of vessels
Volume [µm³]

Figure 6.

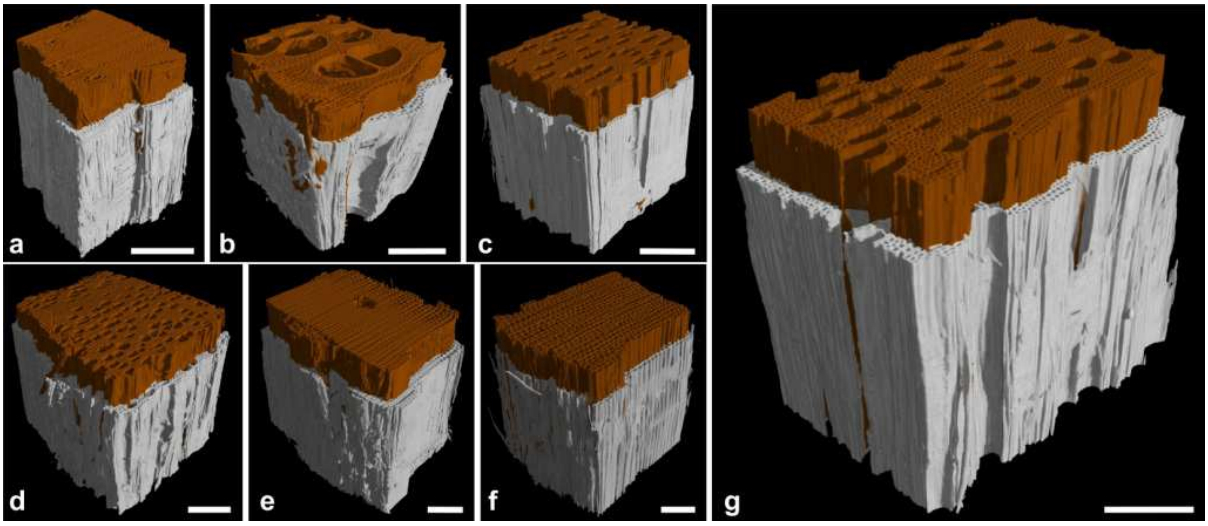

Figure 7.

Figure legends.

Figure 1. Image processing sequence, as exemplified by a reconstructed cross-section of birch wood: original (a), bilateral filtered (b), VOI (c), all cell types labeled (d), vessel lumens labeled (e), cell lumens labeled (f), and 3D rendering of labeled vessel and lumen volumes (g). Scale bar: 200 μm.

Figure 2. Cross sections: ash LW (a), ash EW (b), aspen (c), spruce (d), birch (e), grey alder (f) and pine (g). Scale bar: 200 μm.

Figure 3. Histogram of lumen maximum opening in libriforms (hardwoods) and tracheids (softwoods) before (black) and after (grey) treatment for ash LW (a), ash EW (b), aspen (c), birch (d), grey alder (e), spruce (f) and pine (g).

Figure 4. Histogram of vessel lumen maximum opening before (black) and after (grey) treatment for grey alder (a), aspen (b), birch (c), ash EW (d), and ash LW (e).

Figure 5. Histogram of lumen volume for libriforms (hardwoods) and tracheids (softwoods) before (black) and after (grey) treatment for ash HW (a), ash EW (b), birch (c), aspen (d), grey alder (e), spruce (f) and pine (g).

Figure 6. Histogram of vessel lumen volume before (black) and after (grey) treatment for grey alder (a), aspen (b), birch (c), ash EW (d), and ash LW (e).

Figure 7. 3D renderings of X-ray tomography volumes: ash LW (a), ash EW (b), aspen (c), gray alder (d), pine (e), spruce (f) and birch (g). Untreated samples are grey, and treated specimens are dark brown. Scale bar: 200 μm.